



Numerical modeling of filtration gas combustion in a cylindrical radiation burner for contactless heating of materials

Evgeniy Dats^{a,b,c,*}, Sergey Minaev^{a,c}

^a Department of Computational Informatics, Institute of Applied Mathematics, Radio 7 st., Vladivostok, Russia

^b Vladivostok State University of Economics and Service, Gogolya 41 st., Vladivostok, Russia

^c Far Eastern Federal University, Sukhanova 8 st., Vladivostok, Russia



ARTICLE INFO

Article history:

Received 7 December 2021

Revised 7 June 2022

Accepted 9 June 2022

Keywords:

Filtrational gas combustion

Porous media

Radiative heat losses

Radiative efficiency

ABSTRACT

The filtration gas combustion in a porous cylindrical tube with axial injection of combustible mixture is numerically investigated. This configuration can be potentially used as new type of heater for the contactless heating of materials in industrial processes. The material under treatment is placed inside the cylindrical porous tube and is heated by radiative flux from the cylindrical tube wall. The simulation of the filtration gas combustion in porous burner was carried out within the framework of the two-temperature thermal-diffusion model. Conducted numerical modeling yields qualitative description of the effects of heat removal from the burner on the limits of a stable combustion regime. The data about range of the gas flow rates and the intensity of the heat losses on the burner's inner surface corresponding to the stable combustion were obtained. The temperature distributions in the gas and the porous burner were as well as gas flow field were obtained in general case, without addressing to the details of the material processing.

© 2022 Elsevier Ltd. All rights reserved.

1. Introduction

The filtrational gas combustion in a chemically inert porous media allows create an intensive radiative heat fluxes compared with radiation from free flame. Other advantages of filtrational gas combustion burners over combustion systems with free flame are the higher burning rates, increased power dynamic range, extension of the lean flammability limits, and the low emissions of pollutants [1–3].

Extensive experimental and numerical works were carried out and are still underway, to explore the feasibility of porous burners with filtrational gas combustion for energy production and others applications [4–9]. In the review of Banerjee et al. [10] one can find examples of filtrational gas combustion applications from classical fields like turbines, internal combustion engines, heat exchangers, oil and gas extraction devices to modern areas like food processors, thermoelectric generators, etc. The state-of-the-art experimental, analytical and numerical published studies are surveyed in detail and categorized according to their objectives in review of Ghareghani et al. [11].

Porous radiation burners are promising for creating sources of thermal radiation with controlled power, spectrum and distribution of radiation density for contactless heating of workpieces or materials in industrial processes. The porous radiant burners potentially can be applied in those technical processes where electrical heat sources are used. It can significantly increase production efficiency due to the absence of the electricity generation stage from energy produced by combustion and the transmission electricity losses. Another advantage of porous radiant burners is the insensitivity to the electromagnetic interference and the absence of open flames, reduction of accidents when using lean mixtures, as well as stability of operation and protection from external influences, which is ensured by the gas combustion occurring inside the burner's porous body. Modeling of porous radiant burner can help clarify issues related to burner development, design and performance. To stabilize the flame inside a porous burner, one can use a cylindrical [12,13] or even spherical configuration of burners [14] with a radial inlet of the combustible mixture to the center of the burner. This configuration makes it possible to create a diverging radial gas flow and to stabilize the filtration gas combustion wave inside the porous carcass. This work presents a theoretical study of cylindrical porous burner with axial gas flow. Previously, Wang et al. [15] performed the numerical simulation of combustion in a continuous porous cylindrical burner with axial gas supply. The configuration considered in this paper represents a porous

* Corresponding author at: Department of Computational Informatics, Institute of Applied Mathematics, Radio 7 st., Vladivostok, Russia.

E-mail address: datsep@gmail.com (E. Dats).

Nomenclature

The table of parameters.

parameter	symbol
Temperature of solid phase	T_s
Temperature of gas phase	T_g
Inner radius of the burner	r_1
Outer radius of the burner	r_2
Length of the burner	h
Initial temperature	T_0
Fuel concentration of the lean combustible mixture	Y
Initial fuel concentration of the lean combustible mixture	Y_0
The activation energy	N_a
The universal gas constant	R
The pre-exponential factor	A
The thermal effect of reaction	Q
Heat flux density	H
The thermal conductivity coefficient of solid phase	λ_s
The thermal conductivity coefficient of gas phase	λ_g
Density of solid phase	ρ_s
Density of gas phase	ρ_g
The diffusion coefficient of gas phase	D_c
The average pore size	d_p
The characteristic size of the structural element of the porous media	d_s
The solid medium porosity	ε
Nusselt number	Nu
Heat capacity of solid phase	c_{ps}
Heat capacity of gas phase	c_{pg}
Molar mass of gas phase	M
Permeability of solid phase	k
Dynamic viscosity of gas phase	μ

hollow cylinder with the axial supply of a combustible gas mixture through the end surface of the cylindrical burner. The heated sample is placed in the inner cavity of a cylindrical burner with impermeable to gas walls, which ensures the sample is isolated from interaction with combustion products or a combustible mixture. The outer surface of the porous reactor is thermally insulated. The samples under treatment are heated by radiation from the hot walls of the porous cylindrical burner, inside which the filtration gas combustion wave is stabilized. This scheme of filtration gas combustion can be used to create chemical reactors for contactless heating by radiative heat flux of various materials to high temperatures. Since the inner walls of the hollow cylindrical reactor is impermeable to the combustible mixture or combustion products, the internal cavity in which the sample is placed can be filled with an inert gas or even evacuated to avoid oxidative processes in the heated sample. At the same time, the absorption of the radiation heat flux by the sample can lead to a decrease in the temperature of the inner walls and change the structure of the filtration combustion wave inside the porous cylindrical burner. Therefore, in this work, we set the goal of elucidating the effect of radiation heat losses from the inner walls on the structure of the filtration combustion wave. The limits of stationary combustion wave existence depending on the flow rate of the combustible mixture and other parameters are estimated too.

The numerical simulations of filtrational gas combustion in a porous cylindrical burner is carried out within the framework of a two-temperature thermo-diffusion model [1,3,16] taking into account the gas filtration effects described by Darcy's law. The necessity to separate energy equations for solid and gaseous phases (two-medium or two-temperature model) has been demonstrated, in particular, in the works of Chen et al. [17] and Oliveria et al. [18]. The effects of conduction and radiation, as well as convection of solid with the gas, are incorporated in the solid phase equation. The combustion in a porous medium is described within a two-dimensional model that includes one-step Arrhenius type chemistry, radiative heat losses from the inner surface of hollow cylindrical burner, separate gas and solid energy equations and the

transport of fuel concentration in the case of lean mixture. The typical parameters are chosen close to those previously used in modeling the filtration gas combustion (see, for example, the papers [19,20]). In the review [21], one can find a comparison of the calculated data on the propagation velocity of the filtration gas combustion wave obtained by Zhdanok et al. [19] with experimental data Henneke et al. [20], which showed good agreement. This allows considering that the calculations performed in this work within a similar model have a physical basis and will be capable of describing, at least qualitatively, the experimental phenomena.

2. Mathematical model

In the absence of the local thermal equilibrium between the solid and gas phases, the energy equations for solid and gaseous phases are used separately in modelling of the premixed gas combustion in porous media (two-temperature model).

In the cylindrical coordinates (r, z) these equations read

$$\rho_g c_{pg} \left(\frac{\partial T_g}{\partial t} + u_z \frac{\partial T_g}{\partial z} + u_r \frac{\partial T_g}{\partial r} \right) = \lambda_g \Delta T_g + \rho_g Q W(Y, T_g) - \frac{\alpha}{d_p} (T_g - T_s) \quad (1)$$

$$\rho_s c_{ps} \frac{\partial T_s}{\partial t} = \lambda_s \Delta T_s + \frac{\alpha}{d_s} (T_g - T_s) \quad (2)$$

where T_s, T_g are the temperatures of the porous medium and the gas mixture, respectively. The effects of convection, conduction, chemical energy release due to combustion and the heat exchange with the solid phase are included in the gas phase Eq. (1). The effects of heat conductivity including radiative and conductive heat transfer and heat exchange of solid with the gas are incorporated in the solid phase Eq. (2). Here and below, the subscripts s, g denote the model parameters related to the solid and gas phases, respectively. $\Delta = \frac{1}{r} \frac{\partial}{\partial r} + \frac{\partial^2}{\partial r^2} + \frac{\partial^2}{\partial z^2}$ is the Laplace operator in cylindrical coordinate and $W(Y, T_g) = A \cdot Y \exp(-\frac{N_a}{T_g R})$ is the single-step chemical reaction rate, where Y is the fuel concentration of the lean combustible mixture; N_a is the activation energy; R is the universal gas constant and A is the pre-exponential factor in one-step chemical reaction model. Q is the thermal effect of reaction; λ is the thermal conductivity coefficient, ρ is the density and $\alpha = (\lambda_g Nu) / d_p$ is the heat exchange coefficient related with the Nusselt number Nu and the average pore size d_p . c_{ps} and c_{pg} are the solid and gas heat capacities, respectively. $d_s = d_p(1 - \varepsilon) / \varepsilon$ is the characteristic size of the structural element of the porous media and ε is the solid medium porosity. The equation for fuel concentration reads

$$\frac{\partial Y}{\partial t} + u_z \frac{\partial Y}{\partial z} + u_r \frac{\partial Y}{\partial r} = D_c \Delta Y - W(Y, T_g) \quad (3)$$

where $D_c = \lambda_g / (c_{pg} \rho_g)$ is the diffusion coefficient that is assumed to be equal the gas thermal diffusivity.

Gas flow in a porous medium is described by Darcy's law assuming that the gas flow velocity components u_r and u_z are proportional to the pressure gradients p along the corresponding directions

$$u_r = -\frac{k}{\mu} \frac{\partial p}{\partial r}, \quad u_z = -\frac{k}{\mu} \frac{\partial p}{\partial z} \quad (4)$$

Physically, the pressure drop during the gas motion in a porous medium is associated with the momentum loss due to viscous and dynamic friction. To describe the momentum loss associated with viscous friction, the Darcy model can be used, since the effects of dynamic friction (Forchheimer's equation [22]) are usually applied at high Reynolds numbers $Re \gg 100$. When the Reynolds number

is compared to one, one can prove that pressure drop is a linear function of the velocity, and order of magnitude analysis suggests that this linear dependence may persist for a wide range of Reynolds numbers [22]. The typical values of the Reynolds number are about 100, so for simplicity we used the Darcy equation [23,24].

Darcy's Eq. (4) with the equation of state of an ideal gas

$$\rho_g = \frac{p}{MRT_g} \tag{5}$$

and the equation of continuity form a system of equations describing the gas flow in a porous medium:

$$\frac{\partial \rho_g}{\partial t} = \frac{\partial(\rho_g u_r)}{\partial r} + \frac{\rho_g u_r}{r} + \frac{\partial(\rho_g u_z)}{\partial z} \tag{6}$$

Here k is the permeability of the porous medium, μ is the dynamic viscosity of the gas-air mixture and M is the molar mass of the combustible gas-air mixture.

3. Boundary conditions

Radiation burner made of porous material is a cylinder of length h , with inner and outer radiuses r_1, r_2 , correspondingly. The methan-air mixture is supplied in axial direction through the end of the cylinder $z = 0$. Thermal radiation is emitted by the inner surface of the porous frame $r = r_1$. The outer side surface of the burner $r = r_2$ is thermally insulated. Combustion products exit through the end of the burner $z = h$. The scheme of the porous burner is shown at Fig. 1.

The numerical simulation is carried out in a rectangular computational domain $r_1 \leq r \leq r_2, 0 \leq z \leq h$ with the boundary conditions:

$$z = 0 : Y = Y_0, T_g = T_0, \frac{\partial T_s}{\partial z} = 0, p = p_0 + \Delta p \tag{7}$$

$$z = h : \frac{\partial Y}{\partial z} = 0, \frac{\partial T_g}{\partial z} = 0, \frac{\partial T_s}{\partial z} = 0, p = p_0 \tag{8}$$

Here Y_0 is the initial concentration of the fuel, T_0 is the initial gas temperature, p_0 is the atmosphere pressure, Δp is the pressure difference between the ends of the burner.

Let us assume that in the inner cavity of a cylindrical burner there is a sample with a temperature T_{ref} which creates an axisymmetric radiation flux in the radial direction towards the burner walls.

In this case, the boundary conditions on the inner wall of porous burner are as follows:

$$r = r_1 : \frac{\partial Y}{\partial r} = 0, \frac{\partial T_g}{\partial r} = 0, -\lambda_s \frac{\partial T_s}{\partial r} = \sigma_{sb}(\varepsilon_s T_s^4 - \varepsilon_r T_{ref}^4), \frac{\partial p}{\partial r} = 0 \tag{9}$$

Here σ_{sb} is Stefan-Boltzmann's constant and ε_s and ε_r are the blackness degree of the porous burner wall and the sample surface, correspondingly. In the absence of a sample that absorbs heat, the conductive flux from the burner walls is zero $\lambda_s \partial T_s / \partial r = 0$, and the temperature T_{ref} is equal to the temperature of the inner wall of porous burner $T_{ref} = T_s$. Thus, the T_{ref} determines the level of the radiation heat loss from the inner surface of the burner. The outer side surface of the burner is thermally insulated and it is impermeable for the gas, therefore the all fluxes at this surface are zeros:

$$r = r_2 : \frac{\partial Y}{\partial r} = 0, \frac{\partial T_g}{\partial r} = 0, \frac{\partial T_s}{\partial r} = 0, \frac{\partial p}{\partial r} = 0 \tag{10}$$

Note that the two-temperature model of filtration gas combustion (1-6) with the boundary conditions (7-10) makes it possible to estimate the temperature distribution in a porous burner and

the radiation flux in the inner cavity. Notice, that if the porosity of the solid medium is large and the porous media is transparent for radiation, it is necessary to take into account the radiation transfer between the structural elements of the porous medium [14,25]. In this case, Eqs. (1)–(6) must be supplemented with an equation for the radiation flux density inside the medium. As it was shown in [25] the radiation from the inner layers of the porous body to the ambient in some cases can be even larger than the radiation flux from the surface of the porous burner due to higher temperature of the inner layers of porous matrix. In the papers of Chen et al. [26] and Ferguson et al. [27] it was demonstrated that transport processes and reactions occurring in the pores and at the interfaces significantly affect the performance of the porous media, yet these pore-scale phenomena neglected in the conventional volume averaged models. Accounting of the porous medium discrete structure in the modeling of gas combustion performed at the level of individual pores makes it possible to explain the occurrence of acoustic noise, flame oscillations and to describe the complex dynamics of the filtration gas combustion wave consisting of the individual micro flames [28,29].

The numerical simulations within these models require huge computational resources, therefore, for a qualitative description of the combustion wave behavior in this configuration of a cylindrical burner, the traditional two-temperature model of filtration gas combustion [16] is used. The model allows roughly estimate the radiation fluxes and to clarify the features of filtration combustion wave stabilization.

4. Numerical simulations

The system of Eqs. (1)–(6) with the boundary conditions (7-10) was solved numerically by the finite element method with using of Comsol Multiphysics 5.6 software. The calculation area was divided into two parts and the each part consisted of triangular finite elements. The lower part of the computational region, in which the reaction zone was located, had a size of $0 < z < (h/4)$ and consisted of 1.3×10^6 small triangular elements with the maximum element side 5×10^{-6} m. The mesh size was chosen in such a way that at least five finite elements fit into the chemical reaction zone. To determine the convergence of numerical solution, a set of grids with an element side of 2×10^{-6} m, 5×10^{-6} m and 8×10^{-6} m was used for this region. The flame front position was measured under zero-flux condition on the inner surface for each grid. It was found that the difference between the flame front location for grids with element side 5×10^{-6} m and 8×10^{-6} m is less than 1%, and for grids of 2×10^{-6} m and 5×10^{-6} m the difference is less than 0.05%. Thus it was concluded that the grid size of 5×10^{-6} m is sufficient to observe correct numerical results.

The upper part of the computational domain had a size $(h/4) < z < h$ and consisted of 8.2×10^4 larger triangular elements with the maximum side of the triangular element 5×10^{-5} m. This representation of the computational grid allows to reduce the computational error and speed up the process of finding stationary solutions. The size of the computational domain with smaller triangular elements was chosen from the preliminar simulations showing that the flame was stabilized in the region $(h/15) < z < (h/5)$ where the maximum temperature gradients were observed. At the first stage, for the effective search of the stationary solutions for different parameters of the two-dimensional problem, the temperature distributions of the gas and the porous frame are calculated for zero-flux condition $\partial T_g / \partial r = 0$ at the inner surface of porous burner $r = r_1$. In the absence of the inner heat losses one can use a one-dimensional formulation, when the distributions of temperatures, velocity, pressure, and density depend on the azimuthal coordinate z only. The set of those one-dimensional solutions for the given pressure drops is used as a initial distributions in simulations

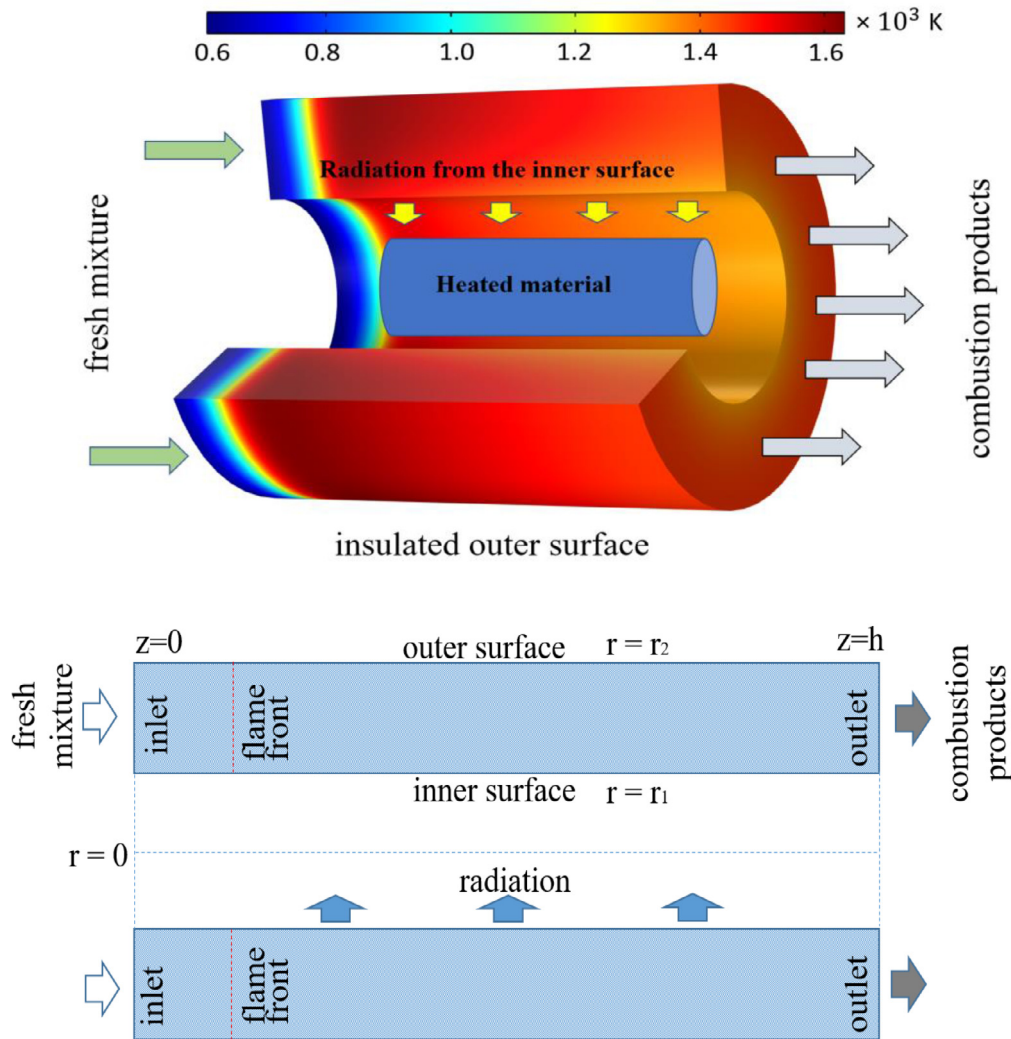


Fig. 1. Scheme of the cylindrical radiant burner with temperature distribution in the porous body. $r_1 = 0.03$ m, $r_2 = 0.06$ m, $h = 0.15$ m.

of the two-dimensional problems taking into account the radiative heat flux from the inner surface of the burner. The burner geometry was set by the following parameters:

$$r_1 = 0.03 \text{ m}, r_2 = 0.06 \text{ m}, h = 0.15 \text{ m}.$$

The properties of the porous nickel-aluminum alloy material were described by the following parameters:

$$dp = 0.001 \text{ m}, \epsilon = 0.5, \lambda_s = 20 \text{ W/(m K)}, c_{ps} = 700 \text{ J/(kg K)}, \rho_s = 2650 \text{ kg/m}^3, k = 25 \cdot 10^{-9} \text{ m}^2, \mu = 2 \cdot 10^{-5} \text{ Pa s}.$$

Preexponential factor A and the activation energy E were fitted so that to roughly approximate the laminar flame speed for the methane-air mixture in the range of equivalence ratios $0.5 < \varphi < 0.8$ at normal conditions. The simulations conducted with the following parameters, corresponding to the methane-air mixture with $\varphi = 0.8$:

$$T_0 = 300 \text{ K}, Y_0 = 0.0445, Nu = 8, \lambda_g = 0.052 \text{ W/(m K)}, c_{pg} = 1200 \text{ J/(kg K)}, M = 0.029 \text{ kg/mol}, p_0 = 10^5 \text{ Pa}, A = 10^9 \text{ s}^{-1}, Q = 42 \cdot 10^6 \text{ J/kg}, N_a = 1.25 \cdot 10^5 \text{ J/mol}, \rho_g = 1.16 \text{ kg/m}^3$$

As it shown in papers Zhang et al. [30,31], the effective heat transfer coefficient in a porous medium is a complex thermophysical parameter determined by the internal structure of a porous medium, radiative heat transfer, and many other factors. The literature uses values of the heat transfer coefficient obtained from experiments both with individual particles and with different particle packings. Experiments with individual particles have shown, for example, that over a wide range of Reynolds numbers, the Nus-

selt numbers measured at the leading edge of a particle with an oncoming gas flow and in the stagnant zone in the tail of a streamlined particle differ by no more than 30-60%. Under filtration conditions, with variable flow directions in the inter-pore space, these variations in heat transfer coefficients smooth out, and the minimum Nusselt number is 2, as in the case of a gas at rest. The typical values of the Nusselt number were chosen similar to that previously used in modeling the filtration combustion of gases [19,20]. The choice of the Nusselt number is due to the semi-empirical dependence for the packing of balls, presented in the work of N. Wakao and S. Kaguie [32]:

$$Nu = 2 + 1.1 \epsilon^{0.6} Re^{0.6} Pr^{1/3} \tag{11}$$

According to this formula, the value of the Nusselt number in the packing of balls varies from 6 to 20 when the Reynolds number changes from 30 to 300 for porosity $\epsilon=0.4$ and $Pr=0.7$.

5. Results

Calculations have shown that in the absence of heat flux from the inner walls of the burner $\partial T_s / \partial r = 0$, the flame front has a flat shape and the flame ring is located perpendicular to the symmetry axis. In the case of heat losses from the inner burner surface, the position and shape of the front change depending on the level of heat losses and the flow rate of the fuel-air mixture.

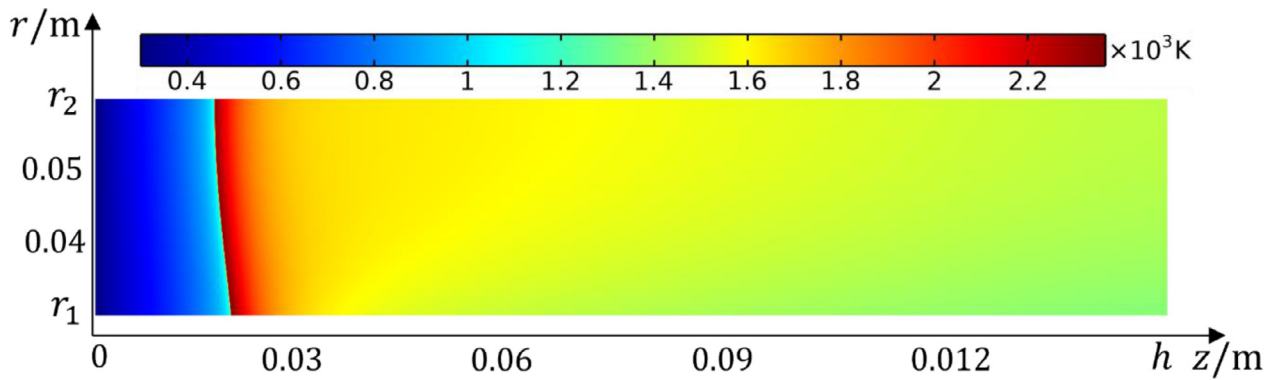


Fig. 2. The gas temperature distribution T_g evaluated at $\Delta p = 1000$ Pa and $T_{ref} = 700$ K.

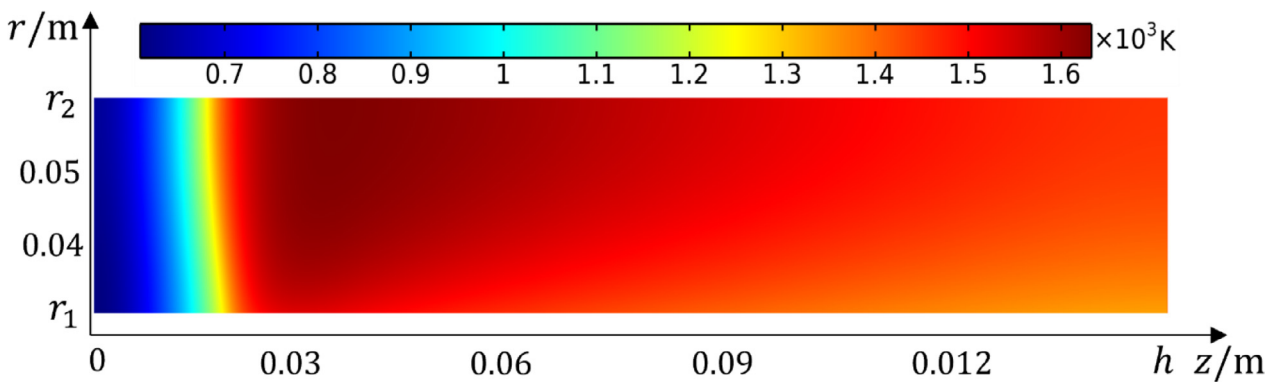


Fig. 3. The porous medium temperature distribution T_s evaluated at $\Delta p = 1000$ Pa and $T_{ref} = 700$ K.

Table 1

Limits of pressure drop values at which a stable combustion mode is observed evaluated for $\varphi=0.8$, $Nu=8$.

$\partial T_s / \partial r _{r=r_1} = 0$	$\Delta p_{min}/\text{Pa}$	min. mass flow rate/(kg/s)	$\Delta p_{max}/\text{Pa}$	max. mass flow rate/(kg/s)	max $T_s(r_1)/\text{K}$
1400	450	0.0073	1150	0.0186	1740
700	650	0.01	1100	0.0178	1590
	800	0.013	1000	0.0162	1534

Stationary solutions exist in a certain range of flow rates of the combustible mixture, determined by the maximum and minimum flow rates of the combustible mixture, which correspond to the maximum Δp_{max} and the minimum pressure drop Δp_{min} at the ends of the burner. At low flow rates of the combustible mixture (small values of the pressure drop $\Delta p < \Delta p_{min}$), the flash back phenomenon occurs, and at high flow rates (large pressure drops $\Delta p > \Delta p_{max}$), the flame is blown out and the combustion wave propagates downstream towards the burner outlet. The level of heat losses is determined by the sample temperature T_{ref} according to the boundary condition (9). There is no heat loss $\partial T_s / \partial r = 0$ if $T_{ref} = T_s$. At lower sample temperatures $T_0 \leq T_{ref} < T_s$, the range of the gas flow rates at which stationary solutions exist is narrowed.

Table 1 shows the maximum and minimum values of the pressure drops depending on the choice of T_{ref} , at which a stable combustion mode is observed. The calculations were conducted for the mixture with equivalence ratio $\varphi=0.8$.

It follows from the Table that as the sample temperature T_{ref} decreases, the range of gas flow rates at which flame stabilization is possible decreases too. Table 2 shows the range of pressure drops of combustible mixture with equivalence ratio $\varphi=0.7$ depending on the choice of T_{ref} . As expected the range of pressure drops corresponding to the stable combustion mode decreases. The values of the minimal and maximal pressure drops Δp_{min} become

smaller than values obtained for mixture with $\varphi=0.8$. This occurs because the normal burning velocity decreases with dilution of the combustible mixture.

The pressure drop limits of stable combustion and the maximal temperature of the inner porous burner surface T_s for different sample temperature T_{ref} determining the level of heat losses by Eq. (9).

Figs. 2 and 3 show the temperature distributions in the gas and in the porous medium, respectively. The calculations were carried out for the values of the pressure drop $\Delta p = 1000$ Pa and the values of the sample temperature $T_{ref} = 700$ K.

At a given pressure drop $\Delta p = 1000$ Pa, the sample temperature $T_{ref} = 700$ K determines the lower temperature limit for the existence of stationary solutions, which exist only at temperatures $T_{ref} \geq 700$ K. Taking into account the axisymmetric formulation of the problem, it follows from Figs. 2, 3 that the filtration gas has the shape of a truncated cone.

The combustion wave front, located closer to the symmetry axis, is farther from the gas inlet into the burner than the wave front located closer to the outer side of the cylindrical burner. This is due to the fact that the temperature of the porous medium layers near the inner wall of the porous burner has a lower temperature than the temperature of the layers near the outer surface of the burner due to radiation losses. At the same time, the temperature of the combustible gas entering the reaction zone re-

Table 2
Limits of pressure drop values at which a stable combustion mode is observed at $\varphi=0.7$, $Nu=8$.

/K	$\Delta p_{min}/Pa$	min. mass flow rate/(kg/s)	$\Delta p_{max}/Pa$	max. mass flow rate/(kg/s)	$max T_s(r_1)/K$
$\partial T_s/\partial r _{r=r_1} = 0$	400	0.0065	950	0.0154	1549
1300	550	0.0089	900	0.0146	1488
600	650	0.0105	800	0.013	1420

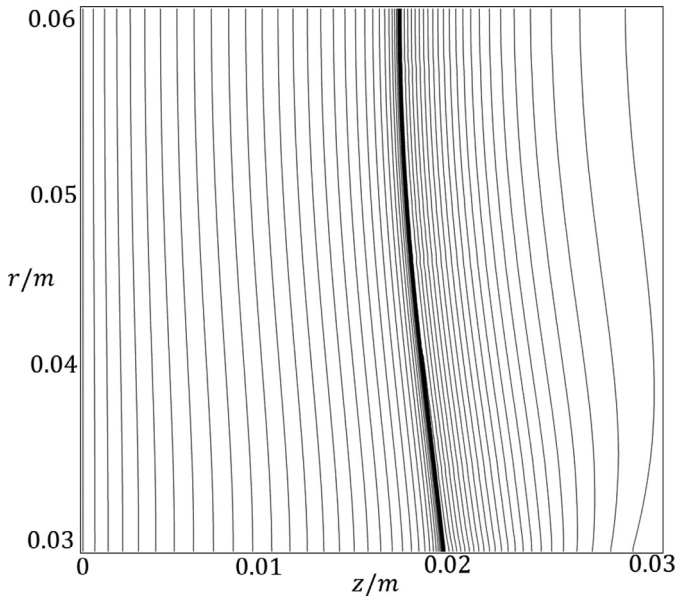


Fig. 4. Lines of the gas temperature level near the combustion wave, corresponding to the calculations shown in Fig. 3. The maximum temperature at the combustion front is 2380 K. Level lines are plotted with a step of 40 K.

mains practically constant along the entire surface of the combustion front, as follows from Fig. 4, on which the gas temperature level lines are plotted corresponding to Fig. 3. The volumes of combustible gas in front of the chemical reaction zone are heated due to heat exchange with a hot porous medium. To heat up to the same temperature of the combustible gas before the start of the chemical reaction, the heating time of gas volumes near the inner wall should be longer than the time for heating the gas near the

outer wall due to the non-uniform distribution of the temperature of the porous medium caused by radiation heat loss. Therefore, the combustion wave form is set so that the combustible gas entering the reaction zone has approximately the same temperature. This interesting effect is associated with the “self-organization” of the filtration combustion wave, which manifests itself in the slope of the combustion wave front.

Calculations have shown that when the sample temperature T_{ref} changes from 700 K to 1200 K, the maximum temperature of the inner wall of the burner changes very weakly and increases by about 30 K. This effect can be explained by the fact that with an increase in the heat loss, the combustion wave changes its shape in such a way as to reduce heat loss into the porous medium from the chemical reaction zone.

Fig. 5 shows the temperature distributions of the gas (dashed line) and the porous frame (solid line) on the outer and the inner surfaces of the burner calculated for a pressure drop $\Delta p = 1000$ Pa and $T_{ref} = 700$ K. The same figure shows the temperature distributions calculated in the absence of the heat losses from the burner inner surface. Note that the maximum gas temperatures in the chemical reaction zone, both near the outer and the inner walls of the burner, are very close to the maximum gas temperature in the reaction zone in the absence of heat losses. This fact is explained by the strong temperature dependence of the chemical reaction rate. The flame propagation is possible only under conditions when the flame temperature differs from the adiabatic temperature of the free flame T_b by a value less than RT_b^2/N_a [33,34].

Fig. 6 shows the temperature distribution in the gas, and Fig. 7 shows the temperature distribution in the porous medium, evaluated for the pressure drop $\Delta p = 1100$ Pa and the sample temperature $T_{ref} = 1400$ K. At a given value of the sample temperature $T_{ref} = 1400$ K, the pressure drop $\Delta p = 1100$ Pa determines the upper limit for the existence of stationary solutions. At large pressure drops, the combustion wave moves along the stream.

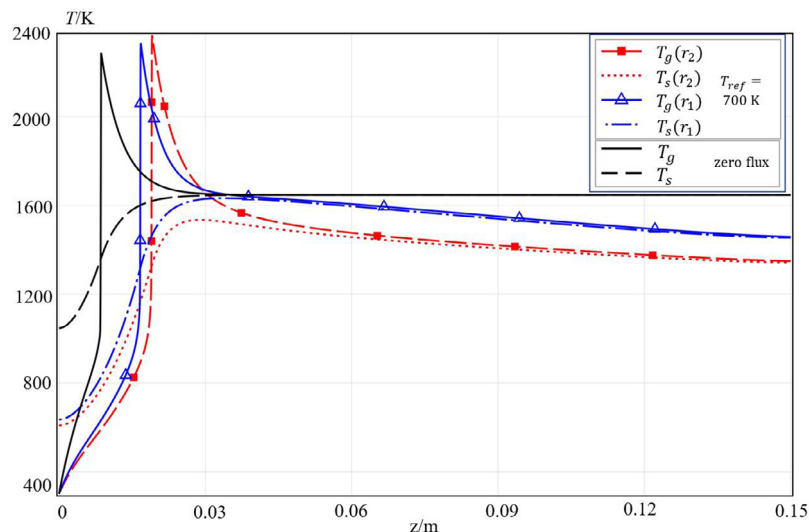


Fig. 5. Temperature distribution of the gas T_g and the porous medium T_s at $\Delta p = 1000$ Pa. $T_{ref} = 700$ K on the inner (red lines) and outer (blue lines) surfaces of the porous burner. The temperature distributions at zero heat flux on the inner surface of the burner are shown by black lines.

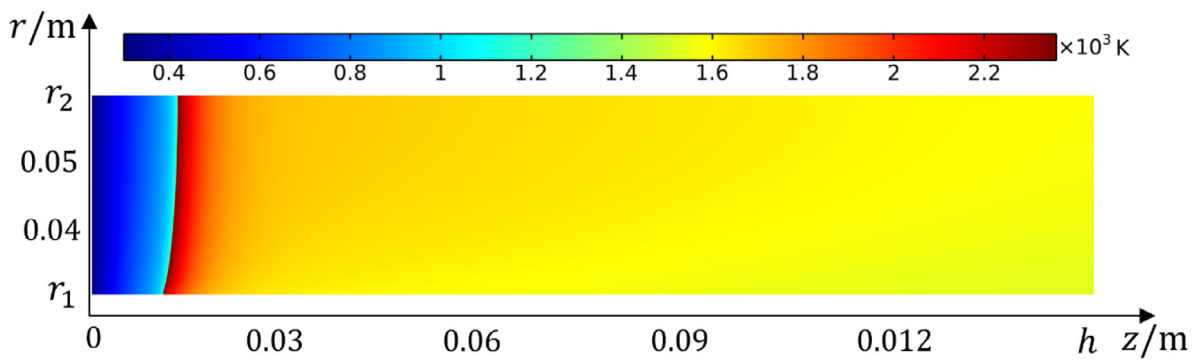


Fig. 6. Gas temperature distribution T_g evaluated for $\Delta p = 1100$ K and $T_{ref} = 1400$ K.

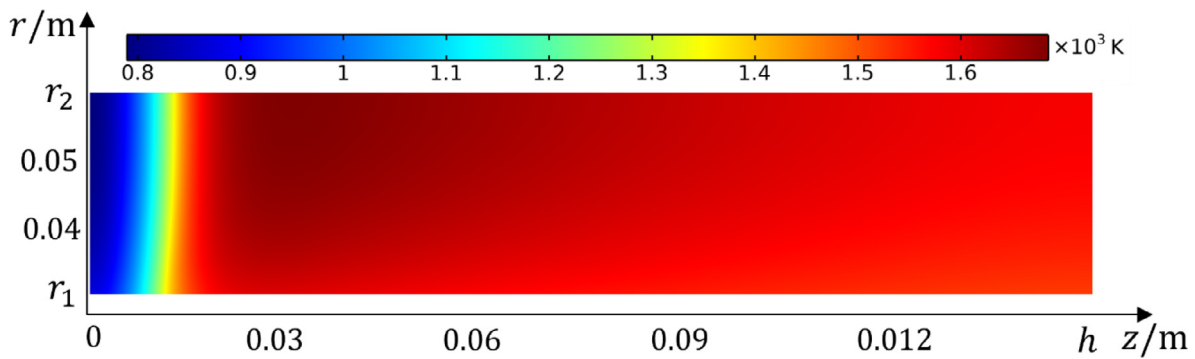


Fig. 7. The porous medium temperature distribution T_s evaluated for $\Delta p = 1100$ Pa and $T_{ref} = 1400$ K.

Figs. 6 and 7 show that the parts of the combustion wave located near the outer wall of the cylindrical burner are farther from the gas inlet to the burner than the parts of the wave located near the inner wall of the burner. At a value of $T_{ref} = 1400$ K, the incoming combustible mixture near the inlet of the burner is heated by the radiation from the hot sample. As a result, the flame shape becomes such that the combustible gas entering the reaction zone has approximately the same temperature. This effect of "self-organization" manifests itself in the curvature of the combustion wave front.

The distributions of the radial u_r and the azimuthal u_z components of the gas velocity for the case under consideration are shown in Fig. 8. The results presented in Figure show that the fresh mixture near the burner inlet moves almost parallel to the axis of symmetry of the burner. Behind the flame front, there is a slight deviation of the velocity vector of the combustion products flow in radial direction. This deviation is caused by the expansion of combustion products behind the curved flame front. Far from the combustion front, in the area of combustion products, the flow becomes homogeneous and moves along the axis of symmetry of the burner.

The upper distribution is radial component of velocity and the bottom distribution is azimuthal component. The right distribution is the velocity vector field plotted for the segment marked by dashed rectangular area.

Fig. 9 shows the distribution of the heat flux densities $H = -\lambda_s(\partial T_s/\partial r)$ from the inner wall of the burner, calculated at $\Delta p = 1000$ Pa, $T_{ref} = 700$ K and $\Delta p = 1100$ Pa, $T_{ref} = 1400$ K.

The maximum value of the heat flux density for the case $\Delta p = 1000$ Pa, $T_{ref} = 700$ K turns out to be approximately 2 times higher than the heat flux calculated for the case $\Delta p = 1100$ Pa, $T_{ref} = 1400$ K. In the case when $T_{ref} = 700$ K the heat flux is directed

from the burner towards the sample ($H > 0$). At a sample temperature $T_{ref} = 1400$ K, the sample gives off heat to the burner ($H < 0$) in the area near the inlet of the combustible mixture, and absorbs heat from the porous framework in the area of combustion products ($H > 0$).

Note that the condition assuming the constancy of the sample temperature T_{ref} is satisfied only in the case of a very high thermal conductivity of the sample material. If part of the sample surface radiates heat to the burner, and the other part absorbs, then the total heat flux entering the sample from the burner must exceed the heat flux from the sample to the burner. Fig. 10 shows the area where the sample transfers heat to the burner (highlighted in blue) and the area where the sample absorbs heat from the burner (highlighted in red). The total area of the red area in Fig. 10, which is proportional to the heat flux from the burner to the sample, is larger than the area of the blue area, which is proportional to the heat flux from the sample to the burner. In this case, no additional heat sources are required to heat the sample.

The choice of the Nusselt number is important factor. According to the formula (11), the value of the Nusselt number in the packing of balls varies from 6 to 20 when the Reynolds number changes from 30 to 300 for porosity $\varepsilon=0.4$ and $Pr=0.7$.

The Fig. 10 shows the temperature distributions of the gas and the porous medium on the inner wall of the burner at the values $Nu = 8$ and $Nu = 12$, evaluated for $\Delta p=800$ Pa, $\varphi=0.7$, $T_{ref} = 600$ K.

It follows from Fig. 10 that with an increase in the Nusselt number, the position of the front shifts closer to the inlet end of the burner. It can be explained by the fact that under conditions of more intensive heat exchange between the gas and the porous medium, the porous medium has a higher temperature behind the front and, as a result, the normal velocity of the flame front increases. Note that the maximum temperatures on the inner sur-

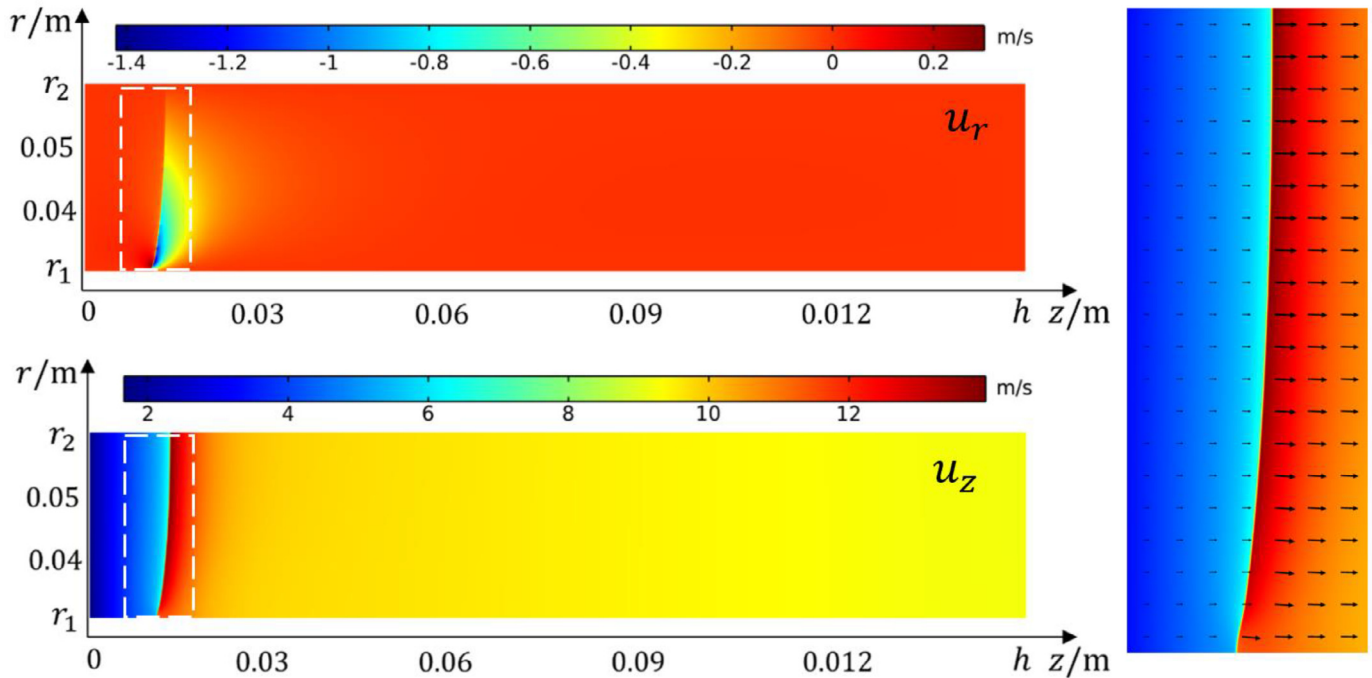


Fig. 8. Components of the velocity u evaluated for $\Delta p = 1100$ Pa and $T_{ref} = 1400$ K.

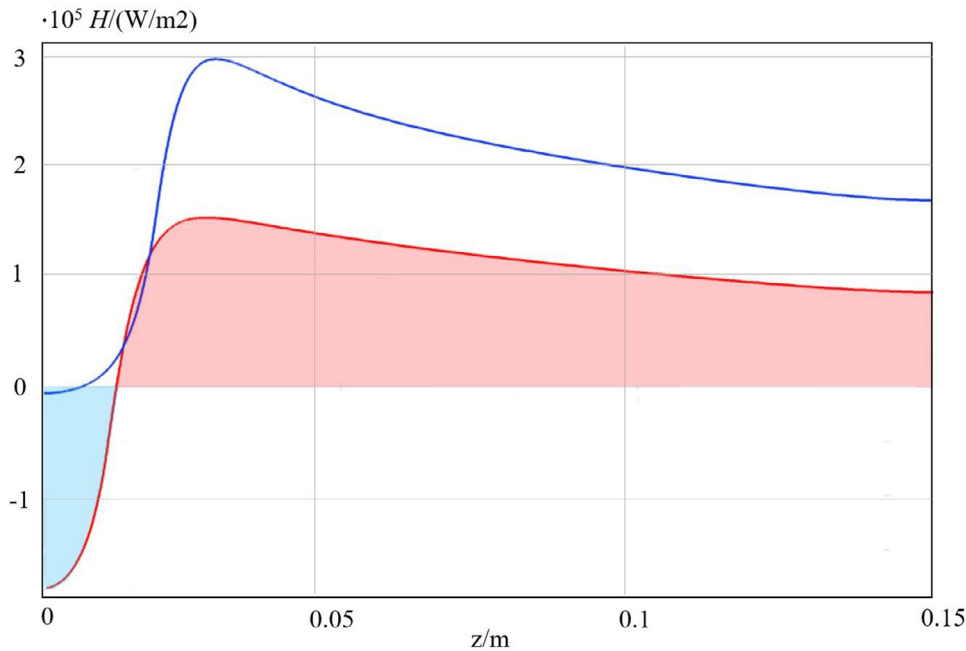


Fig. 9. The heat flux densities H at the inner wall of the cylindrical burner evaluated for $\Delta p = 1000$ Pa and $T_{ref} = 700$ K (blue line), $\Delta p = 1100$ Pa and $T_{ref} = 1400$ K (red line). In the blue area, the sample transfers heat to the burner, and in the red area it absorbs heat from the burner.

face of the frame are almost the same and $T_s = 1420$ K at $Nu = 8$, and $T_s = 1414$ K at $Nu = 12$. Calculations showed that at $Nu = 12$ a stable combustion mode is observed at the maximum possible value of the radiation flux on the inner surface of the burner when $T_{ref} = 300$ K, and the maximum temperature on the inner surface in this case is $T_s = 1412$ K. With a higher heat exchange between the porous medium and the gas (at a higher value of the Nusselt number), the porous burner heats up and reaches the stationary

combustion mode faster. An increase in heat exchange between the porous medium and gas makes it possible to obtain a stable combustion mode at a higher level of radiative heat loss on the surface of the porous medium. It follows from the calculations (Fig. 10) that under the same boundary conditions (heat loss level, pressure drop) for higher values of the Nusselt number, the temperature of the surface is lower than the temperature calculated for a lower value of the Nusselt number.

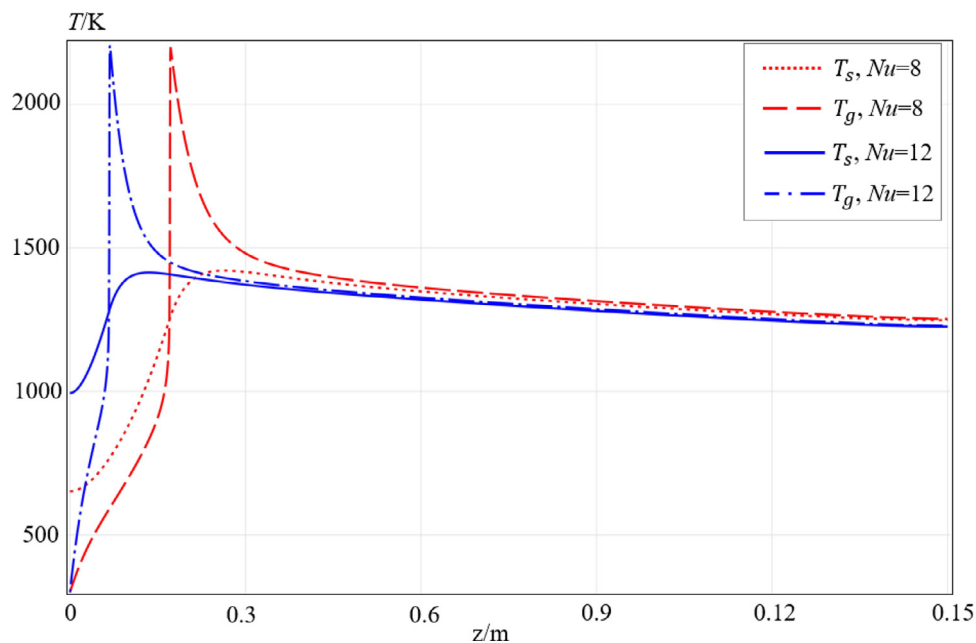


Fig. 10. Temperature distributions of the gas and porous phases on the inner surface of the burner evaluated for $Nu = 12$ (blue lines) and $Nu = 8$ (red lines) and $\Delta p = 800$ Pa, $\varphi = 0.7$, $T_{ref} = 600$ K.

6. Conclusion

The aim of the work was a qualitative description of the effects of heat removal from the burner on the limits of a stable combustion regime and a demonstration of the implementation of such a method of materials heating without additional detailing of the thermophysical properties of the porous medium and the processed samples. The filtration gas combustion in a porous tube with injection of a combustible mixture through the end surface of a porous cylindrical tube is theoretically studied. The simulation of the filtration gas combustion was carried out in the framework of the two-temperature thermal-diffusion model. The influence of the gas flow rate, and the heat losses on the inner surface on the flame stabilization were studied. It was shown that stable combustion can take place in a certain range of pressure drops and radiation heat losses on the burner's inner surface. High levels of radiative heat fluxes and wide range of operation condition with stable combustion shown feasibility of application of this type of porous burners for contactless treatment of different materials. This type of porous radiant burner can be used, for example, as a heat source for the thermal conversion of low-calorie liquid fuels. In this case, the optimization problem can be formulated as achieving the maximum conversion efficiency of the heated fuel. Another potential application may be the creation of a given field of thermal radiation, for various technological processes, for example, in the manufacture of glass. In this case, the optimization problem must take into account the conditions imposed by the applied technologies in order to achieve maximum efficiency. We hope that this work will contribute to the creation of new energy-efficient technologies. Further theoretical and experimental research in this direction will make it possible to formulate and refine a mathematical model depending on the field of application of the proposed type of radiant burner.

Declaration of Competing Interest

The authors declare that they have no known competing financial interests or personal relationships that could have appeared to influence the work reported in this paper.

CRediT authorship contribution statement

Evgeniy Dats: Methodology, Investigation, Formal analysis, Writing – original draft. **Sergey Minaev:** Conceptualization, Supervision, Writing – original draft, Writing – review & editing.

Data availability

No data was used for the research described in the article.

Acknowledgments

This work was financially supported by the [Ministry of Science and Higher Education of the Russian Federation](#) (project No. 075-15-2020-806).

References

- [1] J.R. Howell, M.J. Hall, J.L. Ellzey, Combustion of hydrocarbon fuels within porous inert media, *Prog. Energy Combust. Sci.* 22 (2) (1996) 121–145.
- [2] D. Trimis, F. Durst, Combustion in a porous medium - advances and applications, *Combust. Sci. Technol.* 121 (1-6) (1996) 153–168.
- [3] L. Kennedy, A. Fridman, A. Saveliev, Superadiabatic combustion in porous media: wave propagation, instabilities, new type of chemical reactor, *Int. J. Fluid Mech. Res.* 22 (2) (1996) 1–26.
- [4] A.A. Mohamad, Combustion in porous media: fundamentals and applications, *Transport Phenomena in Porous Media III* (2005) 287–304.
- [5] M.M. Kamal, A.A. Mohamad, Combustion in porous media, a review, *J. Power Energy* 220 (5) (2006) 487–508.
- [6] V.K. Pantangi, S.C. Mishra, Combustion of gaseous hydrocarbon fuels within porous media - a review, *Adv. Energy Res. (AER - 2013)* 455–461.
- [7] S. Wood, A.T. Harris, Porous burners for lean-burn applications, *Prog. Energy Combust. Sci.* 34 (2008) 667–684.
- [8] M.A. Mujeebu, M.Z. Abdullah, M.Z. Abu Bakar, A.A. Mohamad, R.M.N. Muhad, M Khalil, Combustion in porous media and its applications - a comprehensive survey, *J. Environ. Manag.* 90 (2009) 2287–2312.
- [9] M.A. Mujeebu, M.Z. Abdullah, M.Z. Abu Bakar, A.A. Mohamad, M Khalil, Applications of porous media combustion technology - a review, *Appl. Energy* 86 (9) (2009) 1365–1375.
- [10] A. Banerjee, D. Paul, Developments and applications of porous medium combustion: a recent review, *Energy* 221 (2021) 119868, doi:10.1016/j.energy.2021.119868.
- [11] A. Ghareghani, K. Ghasemi, M. Siavashi, S. Mehranfar, Applications of porous materials in combustion systems: a comprehensive and state-of-the-art review, *Fuel* 304 (2021) 121411, doi:10.1016/j.fuel.2021.121411.

- [12] R. Fursenko, A. Maznoy, E. Odintsov, A. Kiryashkin, S. Minaev, S. Kumar, Temperature and radiative characteristics of cylindrical porous Ni–Al burners, *Int. J. Heat Mass Transf.* 98 (2016) 277–284.
- [13] F. Palesskii, R. Fursenko, S. Minaev, *Combust. Explos. Shock Waves* 50 (2014) 625–631.
- [14] K.V. Dobrego, S.A. Zhdanok, S.I. Futko, Effect of porous media transparency on spherical and cylindrical filtration combustion heaters performance, *Int. J. Heat Mass Transf.* 43 (2000) 3469–3480 V– P..
- [15] G. Wang, P. Tang, Y. Li, J. Xu, F. Durst, Flame front stability of low calorific fuel gas combustion with preheated air in a porous burner, *Energy* 170 (2019) 1279–1288, doi:10.1016/j.energy.2018.12.128.
- [16] V.S. Babkin, V.I. Drobushchik, Y.M. Laevskii, S.I. Potytnyakov, Filtration combustion of gases, *Combust. Explos. Shock Waves* 19 (2) (1983) 147–154.
- [17] Y.K. Chen, P.F. Hsu, I.G. Lim, Z.H. Lu, R.D. Matthews, J.R. Howell, Experimental and theoretical investigation of combustion within porous inert media, in: *Proceedings of the 22nd International Symposium on Combustion*, The Combustion Institute, 1988, pp. 22–207. Poster paper.
- [18] A.A.M. Oliveria, M. Kaviani, Nonequilibrium in the transport of heat and reactants during combustion in porous media, *Prog. Energy Combust. Sci.* 27 (2001) 523–545.
- [19] S. Zhdanok, L.A. Kennedy, G. Koester, Superadiabatic combustion of methane air mixtures under filtration in a packed bed, *Combust. Flame* 100 (1–2) (1995) 221–231.
- [20] M.R. Henneke, J.L. Ellzey, Modeling of filtration combustion in a packed bed, *Combust. Flame* 117 (1999) 832–840.
- [21] M. Abdul Mujeebu, M. Zulkifly Abdullah, A.A. Mohamad, M.Z. Abu Bakar, Trends in modeling of porous media combustion, *Prog. Energy Combust. Sci.* 36 (2010) 627–650.
- [22] S. Whitaker, The forchheimer equation: a theoretical development, *Transp. Porous Media* 25 (1) (1996) 27–61.
- [23] M. Kaviani, *Principles of Heat Transfer in Porous Media*, Springer-Verlag, N.Y., 1995.
- [24] L.G. Loitsyanskii, *Mechanics of Liquid and Gases*, 2nd Edition, Pergamon Press, 1966.
- [25] F.S. Palesskii, R.V. Fursenko, S.S. Minaev, Modeling of filtration combustion of gases in a cylindrical porous burner with allowance for radiative heat transfer, *Combust. Explos. Shock Waves* 50 (6) (2014) 625–631.
- [26] L. Chen, A.N. He, J. Zhao, Q. Kang, Z.Y. Li, J. Carmeliet, N. Shikazono, W.Q. Tao, Pore-scale modeling of complex transport phenomena in porous media, *Prog. Energy Combust. Sci.* 88 (2022) 100968, doi:10.1016/j.pecs.2021.100968.
- [27] J.C. Ferguson, S. Sobhani, M. Ihme, Pore-resolved simulations of porous media combustion with conjugate heat transfer, in: *Proceedings of the Combustion Institute*, 38, 2021, pp. 2127–2134.
- [28] R. V.Fursenko, I.A. Yakovlev, E.S. Odintsov, S.D. Zambalov, S. Minaev, Pore-scale flame dynamics in a one-layer porous burner, *Combust. Flame* (2021).
- [29] R. Fursenko, E. Sereshchenko, G. Uriupin, E. Odintsov, T. Tezuka, S. Minaev, K. Maruta, Experimental and numerical study of premixed flame penetration and propagation in multichannel system, *Combust. Sci. Technol.* 190 (6) (2018) 1023–1040.
- [30] G. Zhang, Q. Li, X. Liu, B. Lin, X. Li, Effects of key influencing factors on the flame inclination of low concentration methane (LCM) combustion in porous burner, *Combust. Sci. Technol.* (2022), doi:10.1080/00102202.2022.2054274.
- [31] G. Zhang, Q. Li, X. Liu, B. Lin, X. Li, Numerical investigation on lean methane combustion with modified effective thermal conductivity of the porous media, *Combust. Theory Model.* 26 (2) (2021) 365–382, doi:10.1080/13647830.2021.2017487.
- [32] N. Wakao, S. Kaguie, *Heat and Mass Transfer in Packed Beds*, Gordon and Breach Science publ, 1982.
- [33] D.B. Spalding, A theory of flammability limits and flame-quenching, *Proc. R. Soc. Lond. A* 240 (1220) (1957) 83–100.
- [34] Y.B. Zeldovich, G.I. Barenblatt, Theory of flame propagation, *Combust. Flame* 3 (1959) 61–74.